Available online at www.sciencedirect.com
SCIENCE DIRECT®
International Journal of Heat and Mass Transfer 47 (2004) 2217–2231
International Journal of HEAT and MASS TRANSFER
www.elsevier.com/locate/ijhmt

A pressure based Eulerian–Eulerian multi-phase model for non-equilibrium condensation in transonic steam flow

A.G. Gerber [a,*], M.J. Kermani [b]

[a] Department of Mechanical Engineering, University of New Brunswick, Fredericton, Canada
[b] Department of Mechanical Engineering, School of Engineering, Shiraz University, Shiraz, Iran

Received 19 August 2003; received in revised form 17 November 2003

Abstract

A model for homogeneous nucleation in high-speed transonic flow and applicable to the wet stages of a steam turbine is presented. The model, implemented within a full Navier–Stokes viscous flow solution procedure, employs a pressure based finite-volume/finite-element discretization of the governing equations of fluid motion. Eulerian multi-phase equations, governing both the vapor and liquid phases, are formulated utilizing Classical nucleation theory and the concept of droplet interfacial area density. For the mass conservation of liquid a scalar equation is derived which includes the dispersive motion of the droplets due to turbulent unsteadiness. The solution strategy applies implicit time integration with no constraints on the time-step. Convergence strategies with the highly non-linear homogeneous nucleation process are described. These equations are applied to predict the moisture distribution in low- and high-pressure steam flow in a Laval nozzle and 2D rotor-tip section of a stage turbine.

Keywords: Nucleating steam flow; Computational-fluid dynamics (CFD); Eulerian–Eulerian; Two phase flow

1. Introduction

In the power industry the steam turbine remains an important component for the efficient production of power. The low-pressure turbine stages are of particular interest since they produce the largest portion of the power (across all of the stages), and yet are susceptible to additional losses due to the presence of a second phase. Thermodynamic irreversible losses, generated with non-equilibrium conditions and phase change, are significant to the low-pressure stage efficiency since for every additional percent of wetness the efficiency is reduced by approximately 1% [1] (this estimate of thermodynamic loss, although proposed in 1921, is still in wide use today). Here phase change occurs at high vapor velocities (transonic) and high expansion rates such that the available droplet surface area necessary to bring (or maintain) the flow at near thermodynamic equilibrium must come from a fine mist of droplets formed by homogeneous nucleation.

The modelling of nucleating steam behavior has been ongoing for several decades, and originally was focused on one-dimensional flow in Laval nozzles [2,3], where this geometry was well suited to studying the droplet formation behavior experimentally. However, since the real flow behavior in turbines is considerably more complex more advanced methods for two-dimensional calculations were developed [4,5]. These methods were based on inviscid time marching schemes with a Lagrangian tracking module included to track the particle motion explicitly. To support these models experiments were conducted on 2D blade shapes to verify predicted blade pressure profiles, thermodynamic losses (or efficiencies) and droplet size predictions [6–8]. The Eulerian/Lagrangian approach was further applied to the full Navier–Stokes equations in an approach more closely following multi-phase flow principles [9,10], and included 3D flow calculations for a low-pressure stage.

* Corresponding author.
E-mail address: agerber@unb.ca (A.G. Gerber).

0017-9310/$ - see front matter © 2003 Elsevier Ltd. All rights reserved.
doi:10.1016/j.ijheatmasstransfer.2003.11.017

Nomenclature

a	droplet surface area ($=4\pi r^2$), m^2
c	a non-dimensional constant, Eq. (12)
C	speed of sound, m/s
c_p	specific heat of liquid, or vapor isobaric specific heat, J/kg K
c_v	vapor isochoric specific heat, J/kg K
EOS	equation of state
f	mass fraction of liquid to vapor ($=0.03-0.06$ kg$_f$/kg$_g$), Eq. (38)
h	static enthalpy, J/kg
H	total enthalpy, J/kg
J	nucleation rate, droplet #'s/m^3 s
k	thermal conductivity, W/m K
K	Boltzmann's constant ($=1.3807\times10^{-23}$ J/K)
Kn	Knudsen number, Eq. (12)
m	mass, kg
$Mach$	Mach number
N	number of droplets per unit mass of vapor ($=$droplet #'s/m_g), Eq. (20), droplet #'s/kg$_g$
Nu	Nusselt number ($=2r\lambda/k$)
p	pressure, N/m^2
Pr	Prandtl number ($=\mu c_p/k$)
q_c	condensation coefficient ($=1$ in the present computation)
r	droplet radius, m
r^*	droplet critical radius (droplet radius at nucleation), m
R	gas constant ($=461.4$ J/kg K), or residual for the scalar equation ϕ, Eq. (40)
S	general discrete equation source term, Eq. (39)
S_d	energy equation source term due to viscous dissipation, Eq. (4), W/m^3
S_F	source term for momentum equation with smallest contribution from viscous gradients, Eq. (3), N/m^3
S_h	source term for the interphase energy transfer ($=-S_\alpha h_p$), Eqs. (4) and (29), W/m^3
S_m	source term for the interphase mass transfer ($=-S_\alpha$), Eqs. (1) and (27), kg/m^3 s
S_N	source term for the droplet numbers ($=J$), Eqs. (20) and (26), droplet #'s/m^3 s
S_u	source term for the interphase momentum transfer ($=-S_\alpha u$), Eqs. (2) and (28), N/m^3
S_w	energy equation source term due to useful viscous work, Eq. (4), W/m^3
S_α	source term representing the condensation rate of vapor, Eqs. (19) and (25), kg/m^3 s
S_ϕ	source term of a general scalar equation, Eq. (31)
t	time, s
T	temperature, K
u	velocity, m/s
V	volume of a single control volume, Eq. (31) and Fig. 1, m^3
x	spatial dimension, m

Greek symbols

α	mass fraction of liquid water to water vapor ($=m_f/m_g$), kg$_f$/kg$_g$
β	interfacial area density (sum of interfacial surface areas of all droplets per unit mass of the vapor), m^2/kg$_g$
γ	vapor specific heat ratio
Γ_t	turbulent diffusion coefficient of the liquid scalar equation α, Eq. (19), kg/m s
Γ_ϕ	diffusion coefficient in the discretized equation for a general scalar variable ϕ, Eq. (31)
δ	Kronecker delta function
Δn	outward unit vector of the discrete surface, Eqs. (31) and (32)
Δt	time step, Eq. (31), s
ΔT	integration time interval, Eq. (15), s
ΔG	bulk Gibbs free energy change, Eqs. (6) and (A.4), J/kg
ϵ	turbulent dissipation, m^2/s^3
η	correction parameter, Eq. (8)
κ	turbulent kinetic energy, m^2/s^2
λ	convective heat transfer coefficient, W/m^2 K
μ	dynamic viscosity, kg/m s
ρ	density, kg/m^3
σ	liquid surface tension, N/m
τ	stress, N/m^2
ϕ	general scalar variable ($\in\{1,\alpha,u_i,\text{etc.}\}$), Eqs. (14), (15) and (31)

Subscripts

cv	control volume
eff	effective (laminar + turbulent)
f	fluid (liquid)
g	gas (vapor)
ijk	tensor notation
ip	integration point
nb	neighboring node
p	droplet
P	nodal point
s	saturated state
sc	vapor supercooling, Eq. (9)
t	turbulent

Superscripts

o	property evaluation at old time values, or passive source term of a general scalar equation, Eq. (33)

$\tilde{()}$	Favre-averaging of a scalar variable, Eq. (14)		variable, or active coefficient of general source term, $\partial S_\phi/\partial\phi$, Eq. (33)
$\dot{(\cdot)}$	rate of change of a variable, s^{-1}	$''$	fluctuating term in Favre-averaging of a variable ($()'' = () - \tilde{()}$)
$\overline{()}$	average of a variable, or time-averaging of a conservative variable, Eq. (15)	$\rightarrow$	vector
$'$	fluctuating term in time-averaging of a variable ($()' = () - \overline{()}$), change in dependent		

The approach of coupling the Eulerian phase calculations with explicit droplet integration (i.e. Lagrangian) of the liquid phase suffers when scaling to large three-dimensional flow situations, in particular multi-stage transient flow behavior. For this reason development in the past years has begun to focus on Eulerian/Eulerian schemes for condensing steam flows [11,12]. Such schemes lend themselves more naturally to parallel computing and large transient multi-stage flow calculations. The draw back is the loss in accuracy, since the volumetric averaging of the droplet phase equations leads to a less direct evaluation of particle/vapor behavior, particularly in the region of the nucleation zone where flow conditions change very rapidly. It also will be more challenging to evaluate quantitatively thermodynamic losses since the contribution of the discretization error needs to be more carefully accounted for [13–15].

The contribution of the present paper is that an Eulerian–Eulerian method is presented for homogeneously nucleating viscous turbulent steam flow at transonic conditions, and amenable to low- and high-pressure steam turbines. The method is also unique in that a pressure-based finite-volume/finite-element approach is utilized for the present computation, and an implicit time marching scheme, capable of taking large time steps, is used. The results presented are based on the previous work presented in [9,10], utilizing the same thermodynamic database, and the same computational-fluid dynamics (CFD) solver, but describing a different formulation for predicting moisture.

2. Governing equations

For the presentation of the governing equations, a brief description of conditions leading to droplet formation is required. To begin with homogeneous nucleation in condensing steam occurs at significant levels of supercooling when fluid expansion rates are high. In the case of steam, supercooling levels, defined here as the difference between the local vapor temperature and the saturation temperature (set by the local pressure), in the vicinity of 40 K are achievable. Although heterogeneous droplet formation is active in the flow, the required droplet surface area to achieve reversion to equilibrium can only be obtained with the large number of (very small) droplets created by homogeneous nucleation. The modelling of condensing flows therefore requires properties at supercooled conditions, normally obtained by extrapolation of the vapor equation of state to conditions inside saturation. In addition a theory for nucleation of droplets out of its vapor is required, this is obtained through refinements to Classical nucleation theory.

The fine distribution of droplets, once present in the flow field, require models for the heat and mass transfer between the droplet and vapor phase. Since the droplets appear in the vapor as very small particles (10^{-10}–10^{-9} m), and grow several orders of magnitude in a very short period of time, the heat transfer requires a Knudsen number dependence to cover the free-molecule regime to continuum conditions. The heat transfer following nucleation results in almost all of the latent heat liberated toward the vapor phase. The droplet and vapor temperature both vary approaching saturation conditions.

The two-phase system can be reduced in complexity by employing a no-slip condition between the phases and, for steam, determining the droplet temperature based on capillarity considerations. The details of these assumptions will be discussed subsequently. Applying the assumptions results in a system of equations for the vapor phase, with dependent variables for momentum and mass, u, v, w, p, and for total energy H_g (plus turbulence). Similarly for the liquid phase an equation for mass conservation, with dependent variable α, and for droplet number conservation N. Interaction between the phases is through source terms. The formulation is expressed mathematically in the following sections.

2.1. Vapor phase governing equations

2.1.1. Mass conservation of the vapor phase

A mass conservation equation for the vapor phase then is expressed with a mass source (S_m) to reflect the condensation and vaporization processes present:

$$\frac{\partial \rho_g}{\partial t} + \frac{\partial(\rho_g u_j)}{\partial x_j} = S_m, \tag{1}$$

where ρ_g is the vapor (gas) density and u_j is the j-wise velocity component of the gas. In Eq. (1) a positive S_m corresponds to the case of evaporation, while for the condensation process S_m is negative. The formulation for S_m is given in Section 2.3.

2.1.2. Momentum conservation of the vapor phase

The vapor momentum equations are based on the Reynolds Averaged Navier–Stokes equations (RANS) for three-dimensional turbulent flow, and require a turbulence model to represent the turbulent Reynolds stress terms [16]. The type of turbulence model is not of importance to the condensation model methodology, and the well-established high-Reynolds number κ–ϵ turbulent model is applied in the present case. The influence of turbulence is introduced through an eddy viscosity, which is added to the molecular viscosity to obtain an effective viscosity (μ_{eff}). The momentum equations then appear as

$$\frac{\partial(\rho_g u_i)}{\partial t}+\frac{\partial(\rho_g u_j u_i)}{\partial x_j}=\frac{\partial}{\partial x_j}\left(\mu_{eff}\frac{\partial u_i}{\partial x_j}\right)-\frac{\partial p}{\partial x_i}+S_{F_i}+S_{u_i}, \tag{2}$$

where the source term S_{F_i} contains the smaller terms from the gradient of the Reynolds stress tensor. In general, for compressible turbulent flow S_{F_i} is

$$S_{F_i}=\frac{\partial}{\partial x_j}\left[\mu_{eff}\left(\frac{\partial u_j}{\partial x_i}-\frac{2}{3}\delta_{ij}\frac{\partial u_k}{\partial x_k}\right)\right], \tag{3}$$

where δ is the Kronecker delta function, and the source term S_{u_i} represents the interphase momentum transfer, described subsequently in greater detail.

2.1.3. Energy conservation of the vapor phase

The high-speed energy equation contains source terms representing useful viscous work (S_w) and viscous dissipation (S_d) with the dependent variable the gas total enthalpy (H_g), and has the form

$$\frac{\partial(\rho_g H_g)}{\partial t}+\frac{\partial(\rho_g u_j H_g)}{\partial x_j}=\frac{\partial p}{\partial t}+\frac{\partial}{\partial x_j}\left(k_{eff}\frac{\partial T_g}{\partial x_j}\right)+S_w+S_d+S_h, \tag{4}$$

where T_g is the gas temperature, and k_{eff} the effective thermal conductivity. The total enthalpy is defined as $H_g=h_g+u_i u_i/2+\kappa$, where h_g is the vapor specific enthalpy and κ the turbulent kinetic energy. In Eq. (4), S_w+S_d represents the total viscous stress energy contribution:

$$S_w+S_d=\frac{\partial}{\partial x_j}(u_i\tau_{ij}), \tag{5}$$

where τ_{ij} is the viscous stress tensor. The source term S_h contains the interphase heat transfer to be described subsequently.

2.1.4. Turbulent closures

As already mentioned the turbulence equation employed is the high-Reynolds number κ–ϵ model. The liquid droplets, of sub-micron size, occupy little volume in the flow and on this basis it is assumed that the droplets have no direct influence on the turbulence. However, there is an indirect influence through the velocity field introduced to the κ–ϵ equations in each iteration. The turbulence in the vapor phase does have an influence on the dispersion of the droplets and will be included in the liquid phase equations as shown subsequently. The equations for the turbulence model are not documented here for brevity, but are however well documented elsewhere [17].

2.2. Liquid phase governing equations

The equations describing the liquid phase are simplified by several assumptions particular to condensing steam flows. These are in order:

- The droplets being very small travel at the vapor velocity allowing Eq. (2) to be used for determining the liquid phase velocity. This assumption applies only to the mean velocity field, while instantaneous velocity components of the phases differ leading to turbulent mixing of the dispersed phase.
- The droplets do not appear at high mass fractions therefore the volume occupied by the liquid can be neglected. This justifies not solving volume fraction equations to separate the phases.
- Due to the small sizes of the droplets, their temperature (assumed uniform through the droplet) can be determined by capillarity (i.e. surface tension) conditions eliminating the need for a mass transfer model [18].

2.2.1. Droplet nucleation

The appearance of a second phase (liquid) is governed by the process of homogeneous nucleation [19]. The formation of very fine spherical droplets, with a large cumulative surface area, can only be achieved when a free-energy barrier to forming such droplets is overcome. At large levels of supercooling, for steam in the range of 30–50 K depending on expansion rate, enough droplets are able to pass the free-energy barrier to significantly influence the temperature in the vapor phase. The heat and mass transfer between the released finely dispersed droplets and its vapor brings the flow back to near equilibrium conditions. At these high levels of supercooling the critical droplet radius is very small given by the equation

$$r^*=\frac{2\sigma}{\rho_f\Delta G_g}, \tag{6}$$

where ΔG_g is the bulk Gibbs free energy change of the gas phase and is calculated from the equation of state (see Appendix A), ρ_f is the density of the fluid (liquid) water, and σ is the liquid surface tension. The number of droplets formed is obtained from Classical nucleation theory [19]:

$$J = \frac{q_c}{1+\eta}\left(\frac{2\sigma}{\pi m^3}\right)^{1/2}\frac{\rho_g^2}{\rho_f}\exp\left(-\frac{4\pi r^{*2}\sigma}{3KT_g}\right), \tag{7}$$

where

$$\eta = 2\frac{\gamma-1}{\gamma+1}\frac{h_{fg}}{RT_g}\left(\frac{h_{fg}}{RT_g}-\frac{1}{2}\right) \tag{8}$$

and q_c is a condensation coefficient (generally taken as 1), K Boltzmann's constant, m the mass of one water molecule, and h_{fg} is the equilibrium latent heat. The specific heat ratio and gas constant of the vapor are γ and R, respectively. It should be noted that the choice of surface tension influences the nucleation rate J significantly, and there is debate concerning the validity of using a bulk liquid surface tension (as generally applied) for very small droplet clusters. The surface tension used here is that for bulk water with some adjustments to improve comparison with experiments as outlined in [10].

2.2.2. Droplet temperature

For very small droplets ($r < 1$ μm) the temperature can be determined by the capillarity effects [18] so that

$$T_p = T_s(p) - [T_s(p) - T_g]\frac{r^*}{\bar{r}} = T_s(p) - T_{sc}\frac{r^*}{\bar{r}}, \tag{9}$$

where T_g is the vapor temperature and T_s the saturation temperature at the local pressure p.

2.2.3. Droplet growth rate

From an energy balance around a small spherical droplet undergoing phase change in a pure medium we can estimate the rate of change in the droplet radius beginning with

$$(h_g - h_p)\frac{dm_p}{dt} = a_p\lambda_g(T_p - T_g) + m_p c_{p_f}\frac{dT_p}{dt}, \tag{10}$$

where m_p is the mass of a single liquid droplet ($= 4/3\rho_f\pi r^3$), a_p is the surface area of a single droplet ($= 4\pi r^2$), c_{p_f} is the specific heat of the fluid (liquid), and λ_g is the convective heat transfer coefficient between a liquid droplet and its surrounding (gas).

In Eq. (10) dm_p/dt is the mass condensation (or evaporation) rate over the surface of the droplet, $(h_g - h_p)$ is the local latent heat per unit mass and $(h_g - h_p)dm_p/dt$ is the rate of latent heat to be removed or added. In condensation a part of the latent heat moves toward the vapor via convection, while the remaining portion raises the temperature of the droplet. It is possible to neglect the droplet heating term since this component (for sub-micron droplets) is very small relative to the particle-gas convective heat transfer. This results in a simplified relation of the form

$$4\rho_f\pi r^2(h_g - h_p)\frac{dr}{dt} = 4\pi r^2\lambda_g(T_p - T_g),$$

or more compactly

$$\frac{dr}{dt} = \frac{\lambda_g(T_p - T_g)}{(h_g - h_p)\rho_f}. \tag{11}$$

For the small droplets present from homogeneous nucleation the heat transfer coefficient λ_g must be modified to account for Knudsen (Kn) number effects. A heat transfer coefficient with this dependence, and appropriate for steam, was developed by Gyarmathy [18] with the general form

$$\lambda_g \equiv \frac{Nuk_g}{2r} = \frac{k_g}{r(1+cKn)}, \tag{12}$$

where Nu is the Nusselt number and k_g is the vapor thermal conductivity. The constant c, for this work, is determined on the basis of a model presented by White and Young [4].

2.2.4. Mass conservation of the liquid phase

With the assumption that the volume occupied by the liquid in the mixture control volume is very small, a scalar quantity, α, is used to represent the mass fraction of liquid water to water vapor present in the control volume (i.e. $\alpha \equiv m_f/m_g$). Based on α an equation for the mass conservation of the liquid phase can be developed. Since the flow is turbulent the conservation equation for liquid mass should represent both the mean flow and turbulent dispersion influences on the trajectory of the droplets. To do so we start from an instantaneous equation for the conservation of liquid mass:

$$\frac{\partial(\rho_g\alpha)}{\partial t} + \frac{\partial(\rho_g\alpha u_{f_j})}{\partial x_j} = S_\alpha, \tag{13}$$

where the source term S_α represents the condensation rate of vapor ($S_\alpha > 0$ for condensation), and u_{f_j} represents the liquid phase velocity.

For compressible turbulent flows Favre-averaging of a general scalar variable ϕ, denoted by $\hat{\phi}$, is obtained in the following manner (see [20] for details):

$$\hat{\phi} = \frac{\overline{(\rho_g\phi)}}{\overline{\rho_g}}, \quad \text{where } \phi = \hat{\phi} + \phi'' \tag{14}$$

while the time-averaging of a conservative variable $(\rho_g\phi)$, denoted by $\overline{(\rho_g\phi)}$, is defined by

$$\overline{(\rho_g\phi)} \equiv \frac{1}{\Delta T}\int_t^{t+\Delta T}(\rho_g\phi)\,dt \quad \text{and} \quad (\rho_g\phi) = \overline{(\rho_g\phi)} + (\rho_g\phi)', \tag{15}$$

where $\phi \in \{1, \alpha, u_{f_j}, \text{etc.}\}$, and ΔT is a time interval, an interval assumed long w.r.t. the time scales of turbulence and short w.r.t. those of the mean flow.

In Eqs. (14) and (15) "$\widehat{\ }$" and "$\bar{\ }$" represent Favre- and time-averaging, respectively. With this nomenclature, it can be shown that the time-averaging of Eq. (13) becomes

$$\frac{\partial(\overline{\rho_g}\,\widehat{\alpha})}{\partial t} + \frac{\partial(\overline{\rho_g}\,\widehat{\alpha}\,\widehat{u}_{f_j})}{\partial x_j} = \frac{\partial}{\partial x_j}\left(- \overline{\rho_g \alpha'' u''_{f_j}} \right) + \overline{S}_\alpha. \tag{16}$$

In Eq. (16) $\widehat{u}_{f_j}$ is the Favre-averaged liquid phase velocity, and is taken to be equal to that of the gas phase by assuming no-slip between the phases, i.e.

$$\widehat{u}_{f_j} = \widehat{u}_j. \tag{17}$$

In addition the variable u''_{f_j} represents the fluctuations of the liquid droplet w.r.t. the liquid phase Favre-averaged velocity.

The first term on the RHS of Eq. (16) is similar to the Reynolds stress term in the Reynolds-averaged momentum equations, and can be approximated by using an analogy to the Boussinesq eddy viscosity model so that

$$\left(- \overline{\rho_g \alpha'' u''_{f_j}} \right) = \Gamma_t \frac{\partial \widehat{\alpha}}{\partial x_j}, \tag{18}$$

where Γ_t plays a role similar to the eddy viscosity, and is equal to $\Gamma_t \equiv \mu_t / Pr_t$. The turbulent Prandtl, Pr_t, has a value of 0.9 in the present model.

Finally a scalar equation representing the conservation of the liquid phase, and including turbulent dispersion, is obtained (after dropping "$\bar{\ }$" and "$\widehat{\ }$"):

$$\frac{\partial(\rho_g \alpha)}{\partial t} + \frac{\partial(\rho_g u_j \alpha)}{\partial x_j} = \frac{\partial}{\partial x_j}\left(\Gamma_t \frac{\partial \alpha}{\partial x_j} \right) + S_\alpha. \tag{19}$$

The source term S_α in Eq. (19) is identical to the gas phase source, see Eq. (1), but opposite in sign (i.e. $S_\alpha = -S_m$). All the source terms are described in Section 2.3.

2.2.5. Conservation of droplet numbers

To adequately model the liquid phase the number of droplets is required to estimate the droplet surface area available for heat transfer. The equation for droplet numbers can account for the introduction of droplets at boundaries or by nucleation. The equation is

$$\frac{\partial(\rho_g N)}{\partial t} + \frac{\partial(\rho_g u_j N)}{\partial x_j} = S_N, \tag{20}$$

where N is the number of droplets per unit mass of vapor ($N \equiv \#/m_g$), and the source term S_N ($= J$) is obtained according to the nucleation model of Section 2.2.1.

2.2.6. Auxiliary relations

To help in the development of the interphase source terms, and calculation of important quantities such as droplet size, some auxiliary relations are described here. Through a relationship between α and N, an average droplet mass is obtained as

$$\bar{m}_p = \frac{\alpha}{N}, \tag{21}$$

where $\bar{m}_p = 4/3\pi\rho_f \bar{r}^3$. Therefore, an average droplet radius can be isolated as

$$\bar{r} = \left(\frac{3\alpha}{4\rho_f \pi N} \right)^{1/3}. \tag{22}$$

Calculating the droplet size in this manner assumes the droplet distribution can be adequately represented by an equivalent mono-dispersion of a mean size. If nucleation occurs at other distinct locations in the flow path, perhaps in a subsequent flow expansion, an additional set of equations for α and N would need to be solved to represent an additional droplet size range present.

Along with the average radius a droplet interfacial area density (β) is also defined, which is the sum of the interfacial surface areas per unit mass of the vapor:

$$\beta \equiv N \bar{a}_p = \frac{3\alpha}{\rho_f \bar{r}}, \tag{23}$$

where $\bar{a}_p$ ($= 4\pi\bar{r}^2$) is the average interfacial surface area of a single droplet. Using Eq. (23), an average droplet radius can be alternatively calculated as

$$\bar{r} = \frac{3\alpha}{\rho_f \beta}. \tag{24}$$

2.3. Source terms

Using the solution variables available at the beginning of a new time step, the droplet rate of growth (Eq. (11)), the droplet radius (Eq. (24)) and the droplet interfacial area density (Eq. (23)) can be calculated. Using this information the source terms can be computed as follows:

- *Liquid scalar*. The mass source to the liquid scalar equation, S_α with the units of $[kg_f/(m^3\,s)]$, is obtained by considering the mass growth rate of a droplet of size $\bar{r}$. With N as the total number of droplets per unit vapor mass, the mass condensation rate of all the droplets per unit volume of vapor is obtained by $S_\alpha = \rho_g N \mathrm{d}\bar{m}_p/\mathrm{d}t$. With $N\bar{a}_p$ being the interfacial area of all droplets per unit vapor mass, and using the definition of β, it can be shown that

$$S_\alpha = \rho_f \beta \frac{\mathrm{d}r}{\mathrm{d}t} \rho_g. \tag{25}$$

- *Droplet number*. The source term for droplet numbers is obtained according to the nucleation model, as described in Section 2.2.1.

$$S_N = J, \tag{26}$$

where J has the units [#/(m^3 s)].

- *Vapor mass*. The gas phase source term is equal and opposite to that of the liquid phase, i.e.

$$S_{\mathrm{m}} = -S_\alpha. \tag{27}$$

- *Vapor momentum*

$$S_{u_i} = -S_\alpha u_i. \tag{28}$$

- *Vapor energy*

$$S_h = -S_\alpha h_{\mathrm{p}}, \tag{29}$$

where h_{p} is the enthalpy of a liquid droplet. If the contribution of surface energy is ignored, h_{p} is determined as a function of droplet temperature only. The vapor energy equation source term thus represents the sensible heat related to the droplet temperature rise. The latent heat release to the vapor phase is included implicitly in the definition of the vapor phase enthalpy (i.e. $h_{\mathrm{g}} = h_{\mathrm{f}} + h_{\mathrm{fg}}$), which is incorporated in the total enthalpy, H_{g}.

2.4. Supercooled properties

The evaluation of properties in this model was based on the thermodynamic database for steam by Vukalovich [21]. This database utilizes an equation-of-state (EOS) based on a series of virial coefficients appearing as functions of temperature only, written in the form of

$$p = \rho_{\mathrm{g}} R T_{\mathrm{g}} (B_1 + B_2 \rho_{\mathrm{g}} + B_3 \rho_{\mathrm{g}}^2 + B_4 \rho_{\mathrm{g}}^3), \tag{30}$$

where p, ρ_{g} and T_{g} are pressure, density and temperature of the vapor phase, respectively, and B_1 to B_4 are the virial coefficients described in Appendix A. This EOS was tested for extrapolation into supercooled states at low and high pressures [22]. A detailed description of the thermodynamic database implemented in the present computation is provided in Appendix A.

2.5. Numerical model

The model developed has been implemented within the commercial CFD code CFX-TASCflow. Discretization follows the finite-volume/finite-element approach [23]. The vapor phase conservation equations employed second order discretization, and the solution of the hydrodynamic equations (u, v, w and p) was obtained by a coupled (non-segregated) approach [24,25]. The liquid phase equations experience a sharp discontinuity near the nucleation front and a bounded upwind (first order) scheme was employed for Eqs. (19) and (20). Solutions for all equations are accelerated using an algebraic multi-grid procedure [25]. The solutions presented in this paper were converged to normalized RMS residuals of the order of 10^{-5} or lower and global conservation (normalized by the inflow flux) of 10^{-4} or better (for all conservation equations).

2.5.1. Solution strategy

The liquid and gas phase conservation equations are discretized using a conservative finite-volume integration over a control volume. The discretization of the conservation equations, in the context of a finite-element representation of the geometry, is as follows for a general scalar ϕ:

$$\rho_{\mathrm{g}} V_{\mathrm{cv}} \left(\frac{\phi - \phi^o}{\Delta t} \right) + \sum_{\mathrm{ip}} \dot{m}_{\mathrm{ip}} \phi_{\mathrm{ip}} = \sum_{\mathrm{ip}} \left(\Gamma_\phi \frac{\partial \phi}{\partial x_j} \Delta n_j \right)_{\mathrm{ip}} + S_\phi V_{\mathrm{cv}}, \tag{31}$$

where

$$\dot{m}_{\mathrm{ip}} = (\rho_{\mathrm{g}} \vec{u} \cdot \Delta n)^o_{\mathrm{ip}} \tag{32}$$

and V_{cv} is the volume of the control volume, the subscript "ip" denotes an integration point, the summation is over all the integration points of the surface, Δn is the outward unit vector of discrete surface, Δt is the time step, the superscripts o means property evaluation at the old time level, and $\vec{u}$ is the velocity vector. In Fig. 1 is shown the location of the integration points relative to the flux element and control volume faces.

The source terms relevant to condensation and evaporation for the momentum and liquid scalar equations (Eqs. (25)–(29)) are applied over the control volume, and can be linearized into passive and active terms to promote covergence of the discrete equation set. The linearized source equations can be cast into the general form

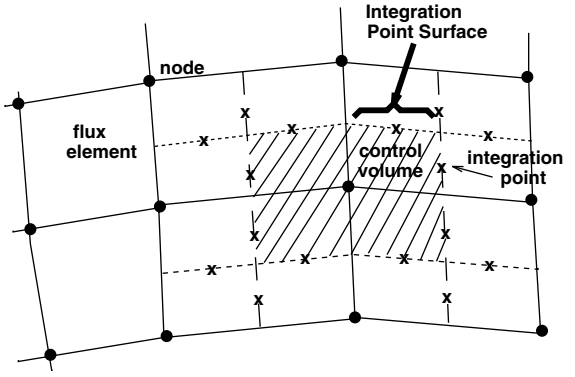

Fig. 1. The location of the integration points relative to the flux element and control volume faces.

$$S_\phi = S_{\phi^o} + S_{\phi'}\phi', \tag{33}$$

where S_{ϕ^o} is the passive source evaluated using old time step values, i.e. ϕ^o, and $S_{\phi'}$ an active coefficient multiplied by changes in the dependent variable (i.e. $\phi' = \phi - \phi^o$). It should be noted that only when negative is the active coefficient applied or else it is assumed zero. This promotes diagonal dominance in the discrete equation set.

The passive source term for the liquid phase α equation is

$$S^o_\alpha = \rho_f \beta \frac{dr}{dt} \rho_g. \tag{34}$$

Similarly the passive source term (for the condensation/evaporation influence) for the i-wise momentum equation becomes

$$S^o_{u_i} = -\rho_f \beta \frac{dr}{dt} \rho_g u^o_i. \tag{35}$$

The active coefficients are obtained by partial differentiation of S_ϕ w.r.t. ϕ (i.e. $\partial S_\phi/\partial\phi$) so that for the liquid scalar

$$S_{\alpha'} = 3\rho_g \frac{dr}{dt} \frac{1}{\bar{r}}. \tag{36}$$

Note that to obtain Eq. (36) the definition for β (see Eq. (23)) was substituted into the formula for S_α and differentiating that w.r.t. α. Similarly the active coefficients of the interphase momentum source terms are

$$S_{u'} = S_{v'} = S_{w'} = -S_\alpha = -\rho_f \beta \frac{dr}{dt} \rho_g. \tag{37}$$

In the case of the energy source no active term is applied since the dependent variable H_g is not present in S_h. Similarly no active term is applied for the droplet number equation.

The present model emphasizes an implicit pressure based solution method. The large times steps that can be employed can lead to very large sources, particularly in the vicinity of the nucleation front. Control of the source is based on utilizing an estimate (from the solution) of the vapor mass flow, ($\dot{m}_g$), through the control volume (either inflow or outflow). The passive part of the liquid mass source term is constrained through the relation

$$S^o_\alpha = \min(\min(S^o_\alpha V_{cv}, f\dot{m}_g), f\dot{m}_g)/V_{cv}, \tag{38}$$

where f is a mass fraction that, when multiplied with the control volume vapor flow, provides a scaled bounding for the mass source S_α. The value of f can be chosen from experimental studies, for example in homogeneous nucleation in nozzles, 3–6% of the mass flow is converted to liquid during the reversion (to equilibrium) process. The lower limit of 3% can be used, since in a reasonably discretized flow domain this amount of mass would not be transferred within a single control volume. The bounding implied in the use of Eq. (38) is only effective during initial start-up of the solution (when a steady-state solution is sought) and disappears within a few time steps as the solution develops. Furthermore the source term, S_α, is heavily relaxed from between iterations, here it was found that relaxation in the vicinity of 0.2 (of the new computed value) was effective. The strategies described here allowed the implicit solution procedure to use time steps much larger than those implied by local CFL limits.

The grid employed hexahedral mesh elements (finite-elements) filling out the domain as shown in Fig. 1, with control volumes derived around the element vertices. Following a finite-volume/finite-element discretization procedure [23], the control volume equations (for scalar equations such as α) can be represented in the general form

$$a_P\phi_P + \sum a_{nb}\phi_{nb} = SV_{cv}, \tag{39}$$

where ϕ_P is the value of ϕ at node P (with a central coefficient a_P), ϕ_{nb} refers to the neighboring nodal values, and a_{nb} the coefficients linking node P to its neighbors. The coefficients include contributions from temporal, convective and diffusive terms.

If the dependent variable is further defined as $\phi = \phi^o + \phi'$, then Eq. (39) can be rearranged into a correction form

$$a_P\phi'_P + \sum a_{nb}\phi'_{nb} = R, \tag{40}$$

where R is a residual that should be reduced to zero at convergence and appears as

$$R = -\left(a_P\phi^o_P + \sum a_{nb}\phi^o_{nb} - SV_{cv}\right). \tag{41}$$

In this context the source term S for the liquid scalar equation ($\phi = \alpha$) appears as

$$S = S_{\alpha o} \tag{42}$$

and the diagonal coefficient term in a_P,

$$a_P = -\sum a_{nb} - S_{\alpha'}V_{cv}. \tag{43}$$

Similar adjustments are made to all governing equations. In the above discussion adjustments to a_P and S for transients has not been included but can be found in [23]. The discrete equations are then solved using an algebraic multi-grid approach [25]. The discrete equations for momentum and mass (or pressure) are coupled and solved directly for the hydrodynamic variables [24]. This by-passes the necessity for segregated iterative procedures such as the popular SIMPLE methods to resolve the pressure–velocity coupling in the flow. The method present here is not limited to a particular approach for resolving the pressure–velocity coupling.

3. Validation

3.1. Laval nozzle with nucleation at low and high pressure [2,3]

To validate the model the first set of test cases consisted of supersonic nozzle flow at high and low pressures. The low-pressure data (below 1 bar) of Moore et al. [2] was used and the results are shown in Fig. 2(Top) for Nozzle A. As is apparent the predicted centreline pressure profile is very good including the condensation shock location, however results for the droplet size are over-predicted. To show that the model predicts important details of homogeneous nucleation Fig. 3(Top) is provided for the low-pressure results. In these results the nucleation event is preceded by supercooling of the vapor phase as shown in parts (a) and (c). The flow wetness only becomes significant after peak nucleation is reached and the vapor temperature returns to near equilibrium as seen in parts (a)–(c). The flow is supersonic in the diverging portion of nozzle, with deceleration of the flow through the nucleation zone as seen by the Mach number profile in Fig. 3(Top) part (d). It should be noted that Mach number profiles in these figures bear the frozen values, which are obtained based on vapor phase speed of sound. The boundary conditions employed for these results were inlet total pressure of 25 kPa and total temperature of 354.6 K.

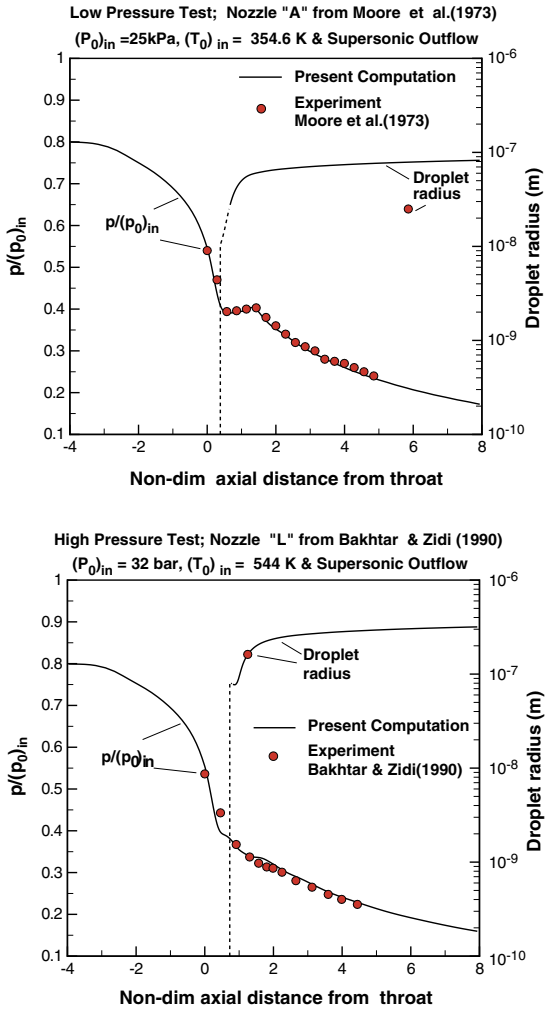

Fig. 2. Comparisons between the proposed model and experiments for centerline pressure and droplet radius. (Top) Low-pressure case, comparisons with nozzle "A" taken from Moore et al. [2]. (Bottom) High-pressure case, comparisons with nozzle "L" from Bakhtar and Zidi [3]. The horizontal axis is non-dimensionalized w.r.t. throat opening.

Since the thermodynamic properties database employed can also be used for high-pressure supercooled steam, a high-pressure nozzle test was also conducted. Using the data (Nozzle L) reported in Bahktar and Zidi [3], a supersonic nozzle with inlet total pressure of 32 bar and total temperature of 544 K was employed. The predicted centreline pressure is compared to the experimental data with good results, and, the droplet radius is very well-predicted at the measured location of 1% wetness fraction. The Wilson point corresponding to these results is 11.3 bar. The maximum supercooling just before nucleation is $\approx$30 K, and is in agreement with the limiting supercooling curve provided by Bahktar and Zidi [3] as a function of Wilson point (11.3 bar) and expansion rate (in this case $\dot{p} \approx 20,000$). The physical features of this test case are shown in Fig. 3(Bottom), parts (a)–(d). Similar behavior to that of the low-pressure (LP) case were obtained with a few highlights explained here. The nucleation rate is much higher in the high pressure (HP) case primarily due to the higher density ratio of the vapor to the liquid (see Eq. (7)). This results in a larger contribution to the source term S_α and, as a result, the wetness fraction in the HP-case is larger than that in the LP-case (see Fig. 3(Top) and (Bottom) part (c) for comparison). In addition, due to the higher density of the vapor in the HP flow, the increased fluid inertia decreases the response (as shown by the Mach number profiles in part (d) of Fig. 3(Top) and (Bottom)) to the condensation front as compared to the LP case.

3.2. Rotor-tip cascade [6]

To test the model in a more complex situation, the rotor-tip experimental data of Bahktar et al. [6] was used for comparison. Fig. 4(Top) shows the blade geometry under study, and the computational domain surrounding the blade, subdivided into seven blocks (grid sizes shown in each block) to provide a grid topology conformed to the blade geometry. Fig. 4(Bottom) shows the grid configuration around the blade, with close-ups near

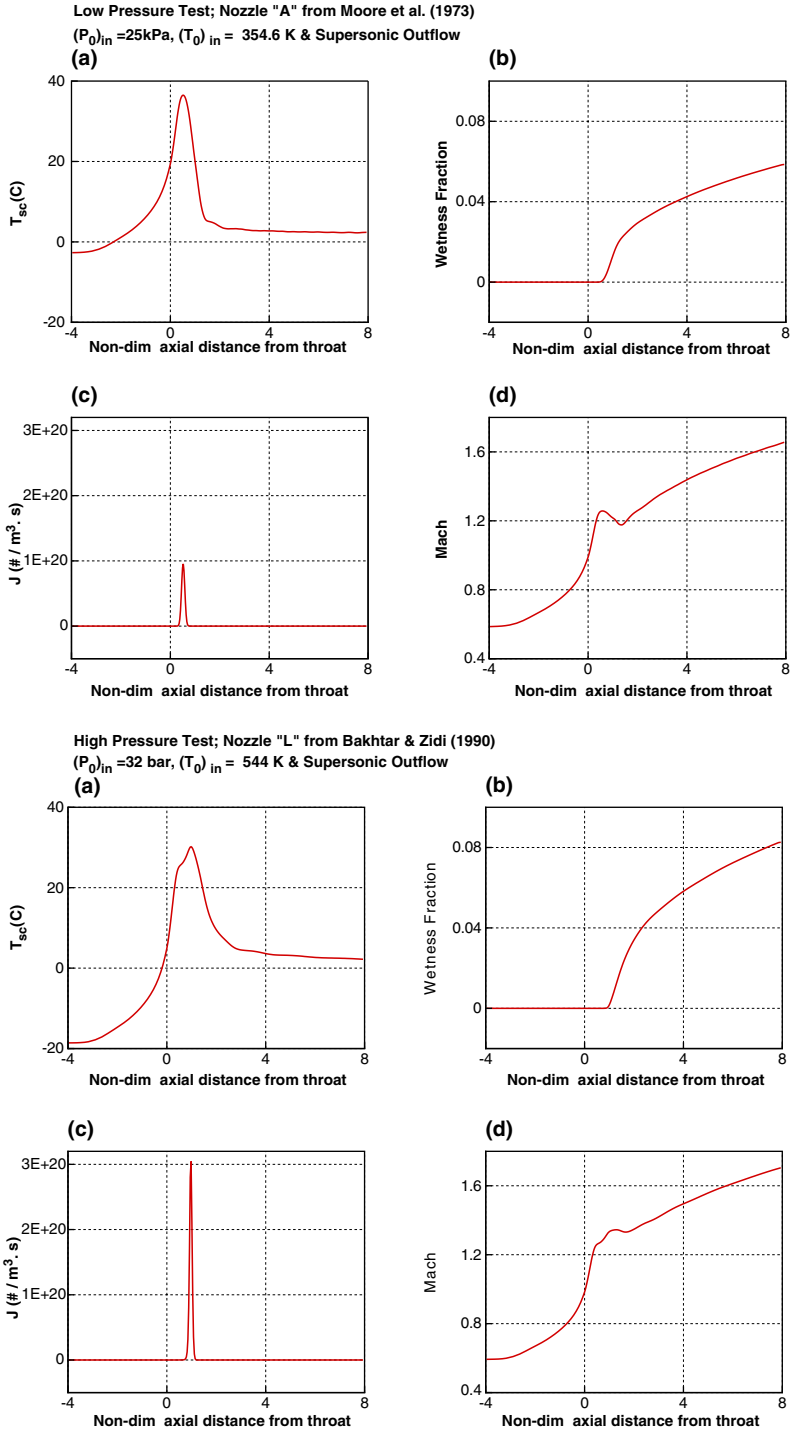

Fig. 3. Centerline values obtained by proposed model. (Top) Results for Nozzle A from Moore et al. [2]: (a) supercooling level, (b) wetness fraction, (c) nucleation rate and (d) frozen Mach number. (Bottom) Similar results with nozzle "L" from Bakhtar and Zidi [3] at high pressure. The horizontal axis is non-dimensionalized w.r.t. throat opening.

the leading and trailing edges of the blade. The case for inlet total conditions of 0.999 bar with 10 K supercooling level at the inlet was employed, with the exit pressure of 0.427 bar.

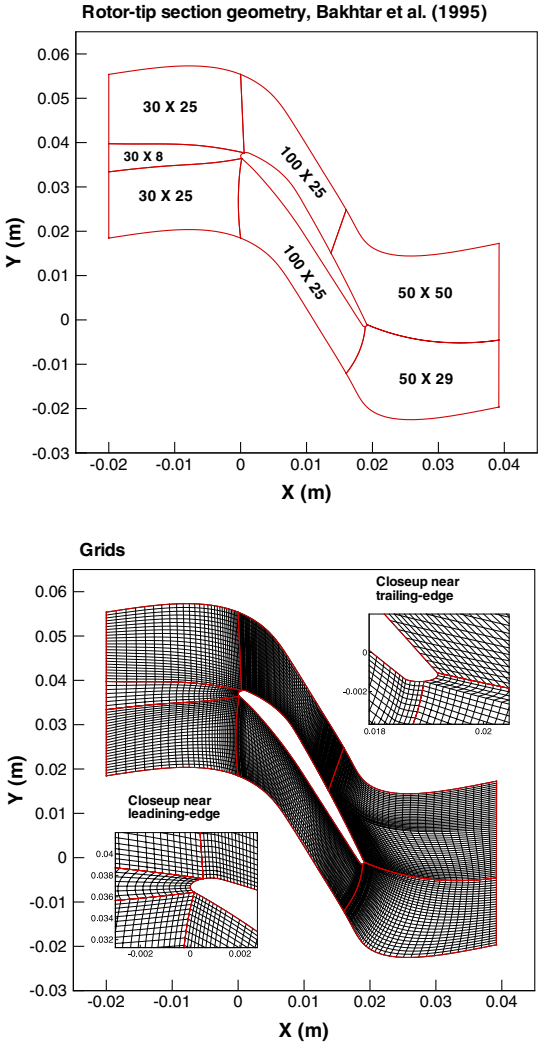

Fig. 4. Geometry of the rotor-tip section: (Top) a multi-block configuration containing seven blocks with the grids in each block shown in the figure and (Bottom) grids used with the close-up near the leading and trailing edges.

The calculated blade pressure profile is compared to experimental values in Fig. 5. The comparison with experiment is good on the pressure side, and the condensation shock along the suction side has been captured reasonably well. However, agreement with data along the suction side near the trailing edge is not so good. The prediction of other features of the flow are shown in Figs. 6–8.

Fig. 6(Top) and (Bottom) shows isobar and iso-Mach lines around the blade. The flow stream of the suction side is subject to a stronger expansion rate as compared to that of the pressure side. As a result, close to the trailing edge a large pressure difference between the pressure and suction sides exists (see Fig. 6(Top)).

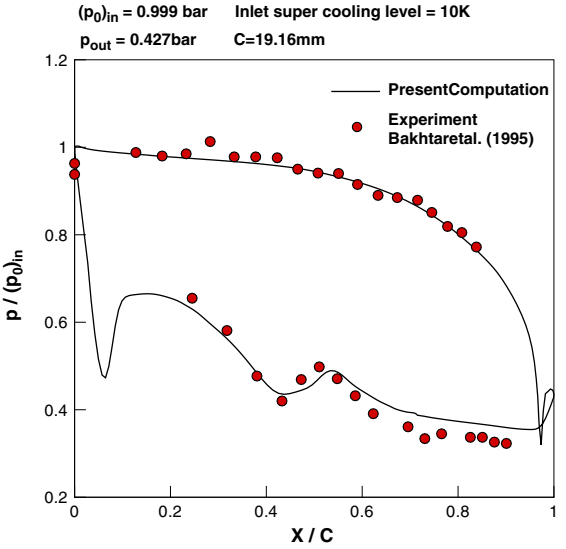

Fig. 5. Rotor-tip cascade, predicted pressure profile vs. experiment.

Beyond the blade both flow streams mix and should come to equilibrium. This requires the suction side stream to pass through a shock, and the pressure side stream to follow an expansion fan beginning at the trailing edge. As shown in Fig. 6, the hydrodynamics of the flow around the blade have been properly captured.

The nucleation rate in the flow is presented in Fig. 7(Top). As is apparent in this figure the nucleation front is captured between the blades, with significant nucleation occurring first along the suction side. The peak nucleation level occurs close to the expansion fan at the trailing edge of the pressure side. Fig. 7(Bottom) shows the supercooling levels. As can be seen supercooling levels increase up to the point just ahead of the nucleation front to a maximum value of ≈45 K. Following nucleation the flow reverts toward equilibrium conditions and supercooling levels decrease. Flow passing through the oblique shock starting from the trailing edge at the suction side, leads to the vapor superheating (negative supercooling indicates superheating) and some evaporation of the liquid present.

The distribution of the liquid in the flow is shown in Fig. 8 via the wetness fraction. As is apparent in this figure the flow remains dry prior to nucleation. Just past nucleation the wetness increases rapidly to ≈3.5% following which wetness levels gradually increase. Partial evaporation of the moisture is also observed through the oblique shock at the suction side of the trailing edge where the wetness fraction reduces from 5% to ≈4%. These flow features are consistent with that obtained by previous studies using different modelling approaches [5,8,9].

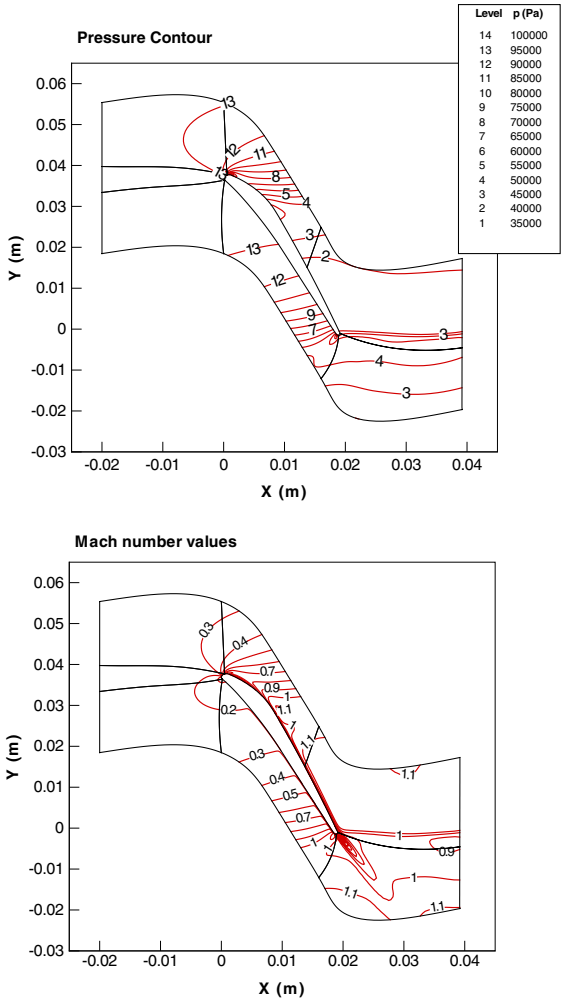

Fig. 6. Rotor-tip cascade: (Top) iso-bar lines and (Bottom) iso-Mach number lines (frozen values, i.e. obtained based on vapor phase speed of sound).

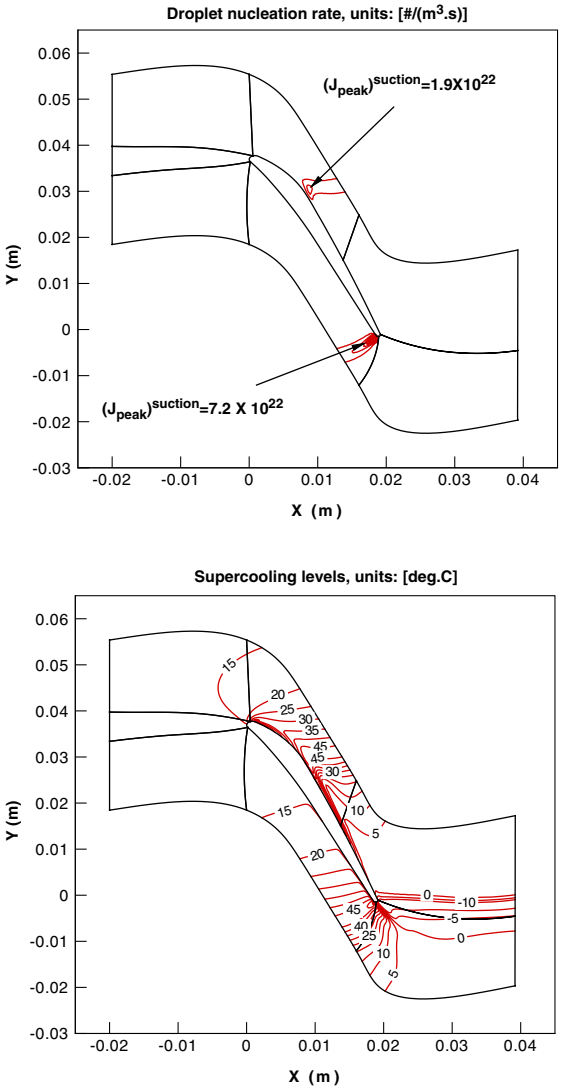

Fig. 7. Rotor-tip cascade: (Top) nucleation front and (Bottom) supercooling levels.

4. Conclusions

An Eulerian–Eulerian multi-phase model has been presented for homogeneous nucleation in transonic turbulent steam flow. The model has been presented in the context of an implicit pressure-based finite-volume scheme applicable to flow at all speeds. Specific handling of source terms for an implicit approach, that can utilize large time-steps in obtaining steady-state solutions (or in transient simulations), is described. Excellent convergence behavior was obtained for all equations on the cases tested, with global conservation 10^{-4} or better (for all conservation equations), and normalized RMS residuals of the order of 10^{-5} or lower.

A scalar equation was presented to model the mass conservation of the liquid droplets, which takes into account the dispersive motion of the liquid droplet w.r.t. vapor phase. A term analogous to the Reynolds stress term appears in this equation ($-\overline{\rho_g \alpha'' u''_{fj}}$) and is modelled based on the Boussinesq eddy viscosity model by substituting $\Gamma_t(\partial\widehat{\alpha}/\partial x_j)$. In conjunction with the liquid scalar equation, a droplet number equation is utilized for estimating the interfacial area density in the flow. The two-phase model was subsequently applied to low- and high-pressure nucleating steam flow in the Laval nozzle and a rotor-tip section. Reasonable agreement with experimental data has been obtained; especially for the pressure distribution. The physical features, typical of flows with homogeneous nucleation, have been captured and compare well with results previously obtained with other numerical schemes.

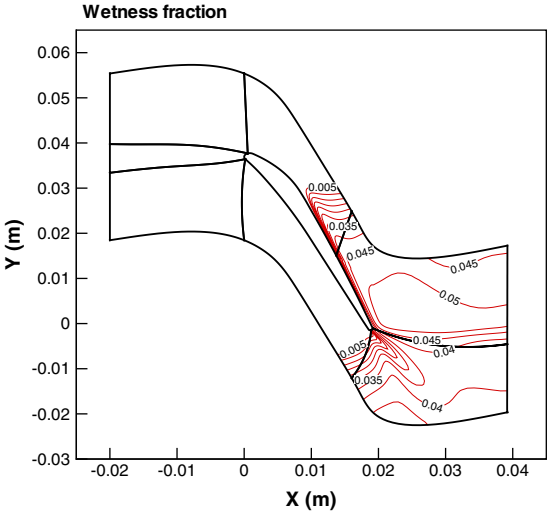

Fig. 8. Rotor-tip cascade, predictions of wetness fraction.

The present model has the potential for efficiently examining large multi-stage turbines where moisture is generated under non-equilibrium conditions. The implicit Eulerian–Eulerian formulation is amenable to efficient parallel execution, and because large time steps can be chosen, difficult transient flow situations can be examined efficiently. In this regard future research will apply the model to 3D rotor-stator stage cases with transient component interactions. Methods will also be examined for calculating cases with a bi-model droplet size distribution. In the present model the droplet distribution is assumed to be adequately represented by an equivalent mono-dispersion of a mean size. This assumption will not be appropriate for 3D models where droplet formation can occur over several stages, including secondary nucleation.

Acknowledgements

The financial support for the present study was provided by the Natural Sciences and Engineering Research Council of Canada (NSERC grant # 238656-01).

Appendix A

For the present non-equilibrium fluid flow calculations the following thermodynamics relationships (in addition to the virial equations of state, given by Eq. (30)) were required for the liquid and vapor phases: specific enthalpy (h), isobaric and isochoric specific heats (c_p and c_v), and speed of sound (C) (only for the vapor phase).

A.1. Superheat state equations

The following equations describe properties in the superheated gas phase and, by extrapolation, information on the gas properties in the supercooled regions of the flow [21,22]:

$$h_g = pv_g - RT_g^2\left(\frac{1}{v_g}\frac{dB_2}{dT_g} + \frac{1}{2v_g^2}\frac{dB_3}{dT_g} + \frac{1}{3v_g^3}\frac{dB_4}{dT_g}\right) + 1.111177T_g + 3.55878\times 10^{-4}T_g^2 - \frac{6991.96}{T_g} + 2070.54, \tag{A.1}$$

$$c_{v_g} = \frac{\partial}{\partial T_g}(h_g - pv_g)_{v_g}, \quad c_{p_g} = c_{v_g} - \frac{T_g(\partial p/\partial T_g)^2_{v_g}}{(\partial p/\partial v_g)_{T_g}}, \tag{A.2}$$

$$C_g = v_g\sqrt{-\frac{c_{p_g}}{c_{v_g}}\left(\frac{\partial p}{\partial v_g}\right)_{T_g}}, \quad R = 461.51\frac{J}{\mathrm{kg\,s}}, \tag{A.3}$$

where v_g ($=1/\rho_g$), is the specific volume of the vapor (or gas), h_g gas enthalpy, p pressure, T_g gas temperature, c_{v_g} and c_{p_g} gas specific heats, C_g gas speed of sound, R gas constant and B_1–B_4 the virial coefficients which are functions of gas temperature only.

The change in the bulk Gibbs free energy of the gas phase (ΔG_g) is also needed to determine the critical radius at which droplets are nucleated. The value of ΔG_g depends on the equation of state used, and for the virial equation of state used in the present computation it is calculated as follows:

$$\frac{\Delta G_g}{RT_g} = -\ln\frac{\rho_g}{\rho_s(T_g)} + 2B_2\{\rho_s(T_g) - \rho_g\} + \frac{3}{2}B_3\left\{\rho_s^2(T_g) - \rho_g^2\right\} + \frac{4}{3}B_4\left\{\rho_s^3(T_g) - \rho_g^3\right\}, \tag{A.4}$$

where $\rho_s(T_g)$ is the saturated vapor density at the local gas temperature T_g, and B_2–B_4 are the virial coefficients.

A.2. Liquid state equations

For non-equilibrium flow calculations with water droplet nucleation properties for the liquid phase are required. When calculating liquid water properties, at saturation, care has to be taken to assure that these properties are consistent with the vapor phase properties at saturation. A reasonably simple approach is to use a saturation curve obtained by experiment, and an empirical liquid density curve as a function of temperature. The liquid properties are assumed not to change with pressure.

With this empirical information available, the liquid properties can then be obtained using the gas phase

equations of state, Eq. (30), and the Clapeyron equation. The resulting relations for the liquid properties are [26]

$$c_{p_{\mathrm{fs}}} = c_{p_{\mathrm{gs}}} - v_{\mathrm{fg}} T_{\mathrm{s}} \frac{\mathrm{d}^2 p_{\mathrm{s}}}{\mathrm{d}T_{\mathrm{s}}^2} - 2T_{\mathrm{s}} \left(\frac{\mathrm{d}p_{\mathrm{s}}}{\mathrm{d}T_{\mathrm{s}}} \right) (\alpha_{\mathrm{g}} v_{\mathrm{g}} - \alpha_{\mathrm{f}} v_{\mathrm{f}}) + T_{\mathrm{s}} \left(\frac{\mathrm{d}p_{\mathrm{s}}}{\mathrm{d}T_{\mathrm{s}}} \right)^2 (\beta_{\mathrm{g}} v_{\mathrm{g}} - \beta_{\mathrm{f}} v_{\mathrm{f}}), \tag{A.5}$$

$$h_{\mathrm{fs}} = h_{\mathrm{gs}} - v_{\mathrm{fg}} T_{\mathrm{s}} \frac{\mathrm{d}p_{\mathrm{s}}}{\mathrm{d}T_{\mathrm{s}}}, \tag{A.6}$$

where $c_{p_{\mathrm{fs}}}$ is the liquid specific heat at saturated temperature T_{s}, $c_{p_{\mathrm{gs}}}$ is the isobaric specific heat of gas at T_{s}, v_{f} specific volume of the liquid, v_{fg} specific volume change of evaporation, p_{s} saturation pressure, and α_{g} and α_{f} are the isobaric coefficient of expansion for the gas and liquid phases obtained from

$$\alpha_{\mathrm{g}} T_{\mathrm{g}} = -\frac{T_{\mathrm{g}}}{\rho_{\mathrm{g}}} \left(\frac{\partial \rho_{\mathrm{g}}}{\partial T_{\mathrm{g}}} \right)_{\mathrm{p}} = \frac{1 + B_2' \rho_{\mathrm{g}} + B_3' \rho_{\mathrm{g}}^2 + B_4' \rho_{\mathrm{g}}^3}{1 + 2B_2 \rho_{\mathrm{g}} + 3B_3 \rho_{\mathrm{g}}^2 + 4B_4 \rho_{\mathrm{g}}^3},$$
$$\alpha_{\mathrm{f}} = -\frac{1}{\rho_{\mathrm{f}}} \left(\frac{\partial \rho_{\mathrm{f}}}{\partial T_{\mathrm{f}}} \right)_{\mathrm{p}}, \tag{A.7}$$

where

$$B_2' = B_2 + T_{\mathrm{g}} \frac{\mathrm{d}B_2}{\mathrm{d}T_{\mathrm{g}}},$$
$$B_3' = B_3 + T_{\mathrm{g}} \frac{\mathrm{d}B_3}{\mathrm{d}T_{\mathrm{g}}}, \tag{A.8}$$
$$B_4' = B_4 + T_{\mathrm{g}} \frac{\mathrm{d}B_4}{\mathrm{d}T_{\mathrm{g}}},$$

and the isothermal coefficient of compressibility, β_{g} and β_{f}, as follows:

$$\beta_{\mathrm{g}} p = \frac{p}{\rho_{\mathrm{g}}} \left(\frac{\partial \rho_{\mathrm{g}}}{\partial p} \right)_{T_{\mathrm{g}}} = \frac{1 + B_2 \rho_{\mathrm{g}} + B_3 \rho_{\mathrm{g}}^2 + B_4 \rho_{\mathrm{g}}^3}{1 + 2B_2 \rho_{\mathrm{g}} + 3B_3 \rho_{\mathrm{g}}^2 + 4B_4 \rho_{\mathrm{g}}^3},$$
$$\beta_{\mathrm{f}} = 0. \tag{A.9}$$

A.3. Required empirical equations

At this point all the necessary properties for the gas and liquid phases have been defined. The reader will note that five empirical equations are required to obtain the preceding equations, namely, the second, third and fourth virial coefficients, the saturation curve and the liquid density curve.

These five equations are now presented beginning with the second, third and fourth virial coefficients (note that $B_1 = 1$), which are functions of gas temperature only [21]:

$$B_2 = -\frac{e}{GT_{\mathrm{g}}} - \phi_1 + b,$$
$$B_3 = -b\phi_1 + 4\phi_1^2 \phi_2, \tag{A.10}$$
$$B_4 = 32 b \phi_1^2 \phi_2,$$

where

$$\phi_1 = \frac{CG}{T_{\mathrm{g}}^{(3+2m_1)/2}}, \quad \phi_2 = 1 - \frac{22.7}{T_{\mathrm{g}}^{(3m_2 - 4m_1)/2}}$$

and

$$e = 63.2, \quad b = 0.85 \times 10^{-3}, \quad C = 0.39 \times 10^6,$$
$$G = 47.053, \quad m_1 = 1.968, \quad m_2 = 2.957.$$

The saturation curve [27]

$$\frac{p_{\mathrm{s}}}{p_c} = \exp \left[\tau 10^{-5} (t_c - t) \sum_{i=1}^{8} F_i (0.65 - 0.01t)^{i-1} \right], \tag{A.11}$$

where

$$\tau = 1000/T_{\mathrm{s}}, \quad t = T_{\mathrm{s}} - 273.15, \quad p_c = 220.88 \text{ bars},$$
$$t_c = 374.136\ ^\circ\mathrm{C},$$
$$F_1 = -741.9242, \quad F_2 = -29.72100,$$
$$F_3 = -11.55286, \quad F_4 = -0.8685635,$$
$$F_5 = 0.1094098 \quad F_6 = 0.439993 \quad F_7 = 0.2520658$$
$$F_8 = 0.05218684.$$

Finally the liquid density as a function of temperature [26] completes the list of empirical equations. Here it is assumed that pressure does not significantly influence the liquid density, which is a valid assumption for wet steam applications.

$$\rho_{\mathrm{f}} = \sum_{i=0}^{3} a_i \tau^i, \tag{A.12}$$

where,

$$\tau = \frac{T_{\mathrm{s}}}{647.286}$$

and

$$a_0 = 928.08, \quad a_1 = 464.63, \quad a_2 = -568.46,$$
$$a_3 = -255.17.$$

The preceding equations defining thermodynamic properties for steam are applicable for equilibrium or non-equilibrium steam calculations, provided superheated conditions are in the range of 0.01–100 bar and 273.15–1000 K. The liquid properties are subject to the constraint that the influence of pressure has been neglected in the liquid density equation.

References

[1] K. Baumann, Some recent developments in large steam turbine practice, J. Inst. Elec. Engrs. 59 (1921) 565.

[2] M.J. Moore, P.T. Walters, R.I. Crane, B.J. Davidson, Predicting the fog drop size in wet steam turbines, in: Wet Steam 4 Conference, Institute of Mechanical Engineers (UK), University of Warwick, 1973, paper C37/73.

[3] F. Bakhtar, K. Zidi, Nucleation phenomena in flowing high-pressure steam, part, 2: theoretical analysis, Proc. Instn. Mech. Engrs. 204 (1990) 233–242.

[4] A.J. White, J.B. Young, Time-marching method for the prediction of two-dimensional, unsteady flows of condensing steam, J. Propul. Power 9 (4) (1993) 579–587.

[5] F. Bakhtar, M.R. Mahpeykar, K.K. Abbas, An investigation of nucleating flows of steam in a cascade of turbine blading—theoretical treatment, ASME J. Fluids Eng. 117 (1995) 138–144.

[6] F. Bakhtar, M. Ebrahimi, R.A. Webb, On the performance of a cascade of turbine rotor tip section blading in nucleating steam, part 1: surface pressure distributions, Proc. Instn. Mech. Engrs. Part C 209 (1995) 115–124.

[7] F. Bakhtar, M. Ebrahimi, B.O. Bamkole, On the performance of a cascade of turbine rotor tip section blading in nucleating steam, part 2: wake traverses, Proc. Inst. Mech. Eng. Part C: J. Mech. Eng. Sci. 209 (1995) 169–177.

[8] A.J. White, J.B. Young, P.T. Walters, Experimental validation of condensing flow theory for a stationary cascade of steam turbine blades, Philos. Trans. R. Soc. Lond. 354 (1996) 59–88.

[9] A.G. Gerber, Two-phase Eulerian/Lagrangian model for nucleating steam flow, ASME J. Fluids Eng. 124 (2002) 465–475.

[10] M.J. Kermani, A.G. Gerber, A general formula for the evaluation of thermodynamic and aerodynamic losses in nucleating steam flow, Int. J. Heat Mass Transfer 46 (17) (2003) 3265–3278.

[11] M. McCallum, R. Hunt, The flow of wet steam in a one-dimensional nozzle, Int. J. Numer. Meth. Eng. 44 (1999) 1807–1821.

[12] S. Senoo, Y. Shikano, Non-equilibrium homogeneously condensing flow analyses as design tools for steam turbines, in: Proc. ASME FEDSM'02, July 14–18, 2002, Montreal, # FEDSM2002-31191.

[13] G.S. Arnold, D.A. Drew, R.T. Lahey Jr., An assessment of multiphase flow models using the second law of thermodynamics, Int. J. Multiphase Flow 16 (3) (1990) 481–494.

[14] J.D. Denton, Loss mechanisms in turbomachines, J. Turbomach. 115 (1993) 621–656.

[15] J.B. Young, The fundamental equations of gas–droplet multiphase flow, Int. J. Multiphase Flow 21 (2) (1995) 175–191.

[16] H. Schlichting, Boundary Layer Theory, seventh ed., McGraw-Hill, New York, 1979.

[17] B.E. Launder, D.B. Spalding, The numerical computation of turbulent flows, Comp. Meth. Appl. Mech. Eng. 3 (1974) 269–289.

[18] G. Gyarmathy, Condensation in flowing steam, in: M.J. Moore, C.H. Sieverding (Eds.), A von Karman Institute Book on Two-Phase Steam Flow in Turbines and Separators, Hemisphere, London, 1976, pp. 127–189.

[19] J.E. McDonald, Homogeneous nucleation of water vapor condensation. I. Thermodynamic aspects, Am. J. Phys. 30 (1962–1963) 870–877.

[20] T. Cebeci, A.M.O. Smith, Analysis of Turbulent Boundary Layers, Academic Press, New York, 1984.

[21] M.P. Vukalovich, Thermodynamic Properties of Water and Steam, sixth ed., Mashgis, Moscow, 1958.

[22] F. Bakhtar, M. Piran, Thermodynamic properties of supercooled steam, Int. J. Heat Fluid Flow 1 (2) (1979) 53–62.

[23] G.E. Schneider, M.J. Raw, Control-volume finite element method for heat transfer and fluid flow using co-located variables, part 1: computational procedure, Numer. Heat Transfer 11 (1987) 363–390.

[24] B.R. Hutchinson, P.F. Galpin, G.D. Raithby, Application of additive correction multigrid to the coupled fluid flow equations, Numer. Heat Transfer 13 (1988) 133–147.

[25] M.J. Raw, A coupled algebraic multigrid method for the 3D Navier–Stokes equations, in: Proceedings of the Tenth GAMM-Seminar, January 14–16, Kiel, Germany, Notes on Numerical Fluid Mechanics, vol. 49, Vieweg-Verlag, Braunschweig, Wiesbaden, 1995.

[26] J.B. Young, An equation of state for steam for turbomachinary and other flow calculations, J. Eng. Gas Turbines Power 110 (1988) 1–7.

[27] J.H. Keenan, F.G. Keyes, P.G. Hill, J.G. Moore, Steam Tables: Thermodynamics Properties of Water Including Vapor, Liquid and Solid Phases, John Wiley & Sons, New York, 1978.